

Measurements and Modeling of Human Blockage Effects for Multiple Millimeter Wave Bands

Wenzhe Qi¹, Jie Huang¹, Jian Sun^{1,2}, Yi Tan³, Cheng-Xiang Wang^{1,3}, and Xiaohu Ge⁴

¹Shandong Provincial Key Lab of Wireless Communication Technologies, Shandong University, Jinan, Shandong, 250100, China.

²State Key Lab. of Millimeter Waves, Southeast University, Nanjing, 210096, China.

³Institute of Sensors, Signals and Systems, School of Engineering & Physical Sciences, Heriot-Watt University, Edinburgh, EH14 4AS, U.K.

⁴School of Electronic Information and Communications, Huazhong University of Science and Technology, Wuhan, 430074, China.

Email: qiwenzhe67@163.com, hj_1204@sina.cn, sunjian@sdu.edu.cn, yi.tan@hw.ac.uk, cheng-xiang.wang@hw.ac.uk, xhge@mail.hust.edu.cn

Abstract—This paper investigates the blockage loss caused by human body at 11, 16, 28, and 32 GHz by measurements and modeling. The measurements are carried out in an office environment by using a vector network analyzer (VNA) and two horn antennas, with one or two persons walking along or across the line connecting the transmitter (Tx) and receiver (Rx). The METIS knife-edge diffraction (KED) model, Kirchhoff KED model, and geometrical theory of diffraction (GTD) model are used to simulate the human blockage effects. The Gaussian model is also used to fit the measurement data. The human blockage effects are compared for the four millimeter wave (mmWave) bands. The results have shown that as the frequency increases, there is no obvious increasing trend of the losses. The METIS KED model, Kirchhoff KED model, and GTD model can simulate the human blockage effects well.

Index Terms—5G, millimeter wave, human blockage effect, KED, GTD.

I. INTRODUCTION

With the development of wireless communication systems, we are now facing the shortage of the frequency resource below 6 GHz [1], [2]. Due to the large bandwidths to provide high data rate transmission, mmWave communication has been a key technology for the fifth generation (5G) wireless communication [3], [4]. MmWave is likely to be used for indoor scenarios due to the large bandwidths and high attenuation. For indoor wireless communication, the height of Tx is low, and the transmit power is small, especially for mmWave bands, thus the blockage effects caused by human body in the environment will be severe.

The human blockage effects have been investigated at some mmWave bands. In [5], 26 and 39.5 GHz measurements were conducted by using a time domain channel sounder and horn antennas. They measured the blockage attenuation when one to three persons walked frontal and lateral crossing the Tx–Rx connecting line or when a person walked along the Tx–Rx connecting line. The Vogler’s multiple KED model was used to model the blockage effects. The loss at 26 GHz was found smaller than that at 39.5 GHz. In [6], a human blockage model was presented on the basis of ray tracing simulations, a diffraction model, and a random walk model. In [7], a wideband channel sounder was used to measure human blockage effect at 60 GHz. The KED model and uniform theory of diffraction (UTD) model were used to do the simulations. In [8], 60 GHz measurements were conducted by using a VNA and two 20 dBi horn antennas. They measured the blockage effects caused by a human leg, a plastic cylinder filled with water or wrapped with aluminum foil, and a thin metallic sheet. Results showed that blockage effect caused by a plastic

cylinder filled with water or wrapped with aluminum foil agreed better than the metallic sheet with the human leg. The GTD model was used to simulate the blockage caused by a cylinder wrapped with aluminum foil. The loss at 60 GHz ranged from 0 dB to –35 dB. In [9], 60 GHz time domain measurements were conducted to obtain a complete statistical description of received power levels. The results were analyzed by using an additive model. In [10], 73 GHz measurements were conducted by using a time domain wideband correlator channel sounder and 20 dBi horn antennas. They measured the blockage effects when a person walked across the Tx–Rx connecting line. The modified METIS KED model was used to simulate the blockage effects. The loss caused by human blockage at 73 GHz was found to be in the range of 30–40 dB.

For KED method, the human body is modeled by a rectangular absorbing screen. For GTD method, the human body is modeled by a perfectly conducting cylinder. Meanwhile, as shown in [11], the blockage caused by human body presented a Gaussian-like shape. The Gaussian shape can simulate the maximal shadowing attenuation in decibels and the shadowing duration in seconds.

In this paper, we carry out the human body blockage measurements at four mmWave bands, i.e., 11, 16, 28, and 32 GHz, by using a VNA and two 20 dBi horn antennas in an indoor office environment. The measurements include three cases: (1) One person walks along the Tx–Rx connecting line; (2) One person walks across the Tx–Rx connecting line; (3) Two persons walk across the Tx–Rx connecting line. The KED and GTD models are used in the simulation, and the Gaussian model is used to fit the measurement data.

The rest of the paper is organized as follows: Section II describes the human blockage measurement environment and system setups. Section III describes the KED Model, GTD Model, and Gaussian-like Model. Measurement and simulation results for human blockage effects are compared and analyzed in Section IV. Finally, conclusions are drawn in Section V.

II. HUMAN BLOCKAGE MEASUREMENTS

The human blockage measurements are conducted in an indoor office environment with room size of $7.2 \times 7.2 \times 3 \text{ m}^3$, as shown in Fig. 1(a) [12]–[15]. The room is furnished with multiple chairs, desks and tables. The layout of the office is shown in Fig. 1(b). The Keysight N5227A VNA is used to do the measurements. The measurements are conducted at four mmWave bands, i.e., 11, 16, 28, and 32 GHz. For each band, the measurement bandwidth is 2 GHz, and two 20 dBi horn antennas are used. The number of frequency sweeping points

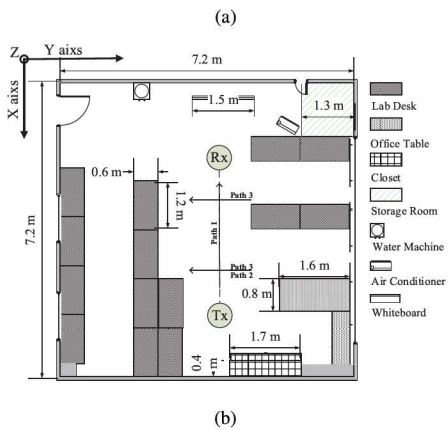


Fig. 1. (a) Photo of the office environment and (b) layout of the office.

is 401. The Tx and Rx antenna are aligned with both heights of 1.4 m. At first, the received signal power with no blockage is measured and denoted by L_0 . Then we measure the received signal power with one or two persons walk along or across the Tx-Rx connecting line, denoted by L_s . Thus the loss caused by human blockage is $L(dB) = L_0 - L_s$. Three cases of the human blockage measurements will be presented in detail in Section IV.

III. HUMAN BLOCKAGE MODELS

Most of researches on human blockage effects use the rectangular absorbing screen or perfectly conducting cylinder to simulate the human body. The KED and GTD models are the most widely used. In this paper, the Gaussian model is also used to fit the measurement data.

A. KED Model

The KED model assumes a human blocker to be represented as a rectangular screen which has an absorbing property. Two KED models are often used to calculate the losses caused by the human blockage effects. The first method is a numerical approximation developed by the METIS project, which is called the METIS KED model in this paper. The second method uses the Kirchhoff diffraction equation to calculate the losses caused by the human blockage effects, which is called the Kirchhoff KED model.

1) *METIS KED Model*: The METIS KED model [16] can calculate the loss caused by human blockage simply and accurately [17]. As is shown in Fig. 2(a), a rectangular absorbing screen is used to simulate the human body. The screen is vertical to the ground and the screen orientation is parallel to the projection of the Tx-Rx connecting line in the top projection view. The four edges of the screen are used to calculate the loss, i.e., the edges on the left, right, top, and bottom. The attenuation caused by the top edge (A_t) and the attenuation caused by the bottom edge (A_b) are calculated by using the

side projection view of the screen. Meanwhile, the attenuation caused by the left edge (A_l) and the attenuation caused by the right edge (A_r) are calculated by using the top projection view of the screen.

If the heights of the Tx and Rx antennas are not the same, then the line connecting the Tx and Rx is not vertical to the screen in the side projection view. The attenuation caused by each edge of the rectangular absorbing screen is calculated by using the following equation [16]:

$$A = \frac{\text{atan}\left(\pm \frac{\pi}{2} \sqrt{\frac{\pi}{\lambda}(D_1 + D_2 - D)}\right)}{\pi} \quad (1)$$

where λ is the wavelength corresponding to the carrier frequency. In a certain projection view shown in Fig. 2, D_1 is the projection distance from the edge to the Rx antenna, D_2 is the projection distance from the edge to the Tx antenna, D is the projection distance from the Tx to the Rx, w is the shoulder breadth of the blocking person, and h is the height of the person. The \pm sign in the equation refers to two cases of the blockage effect. In the case that there is no line of sight (LOS) path exists in the projection view, the plus sign is chosen for the two edges to calculate the attenuation. When a LOS path exists in the projection view shown as Fig. 2(d), the plus sign is chosen for the edge farther from the LOS path, and the minus sign is chosen for the nearer edge.

After the calculation of the attenuation caused by each edge of the screen, the total loss is obtained by [16]:

$$L(dB) = -20 \log_{10}(1 - (A_l + A_r)(A_t + A_b)). \quad (2)$$

One of the merits of the METIS KED model is that it can model the losses when the signal is blocked by several persons simultaneously. When the distribution of the persons is sparse, the total loss is summation of the multiple screens whose loss can be calculated as mentioned above. When the distribution of the persons is dense, the total loss is modeled as the summation of two parts: the loss due to the dominating shadowing screens and the loss due to the multiple screens in the middle.

The loss caused by the screen nearest to Tx antenna, nearest to Rx antenna, and at the middle are denoted by L_{tx} , L_{rx} , and L_{mid} . If the Tx and Rx are both lower than the multiple screens, then the dominating shadowing screens are the ones which is nearest to the Tx or Rx antenna. The loss L_{tx} and L_{rx} can be calculated by using the method mentioned above to calculate the loss due to a screen.

2) *Kirchhoff KED Model*: In the Kirchhoff KED model [18], [19], the Kirchhoff diffraction equation is used to simulate loss caused by human blockages. Fig. 3 shows the aperture diffraction for the Kirchhoff KED model. As shown in Fig. 3, S is a screen extended infinitely in the X-Y plane, S_0 refers to the aperture on the screen, Q_0 is the intersection point of the Tx-Rx connecting line with the aperture, d_1 and d_2 denotes the projection of Tx- Q_0 and Rx- Q_0 on Z axis, respectively.

The first Fresnel zone radius can be calculated as

$$R_1 = \sqrt{\lambda \frac{d_1 d_2}{d_1 + d_2}} \quad (3)$$

The attenuation caused by the aperture can be calculated using the Kirchhoff diffraction equation [18] [19]:

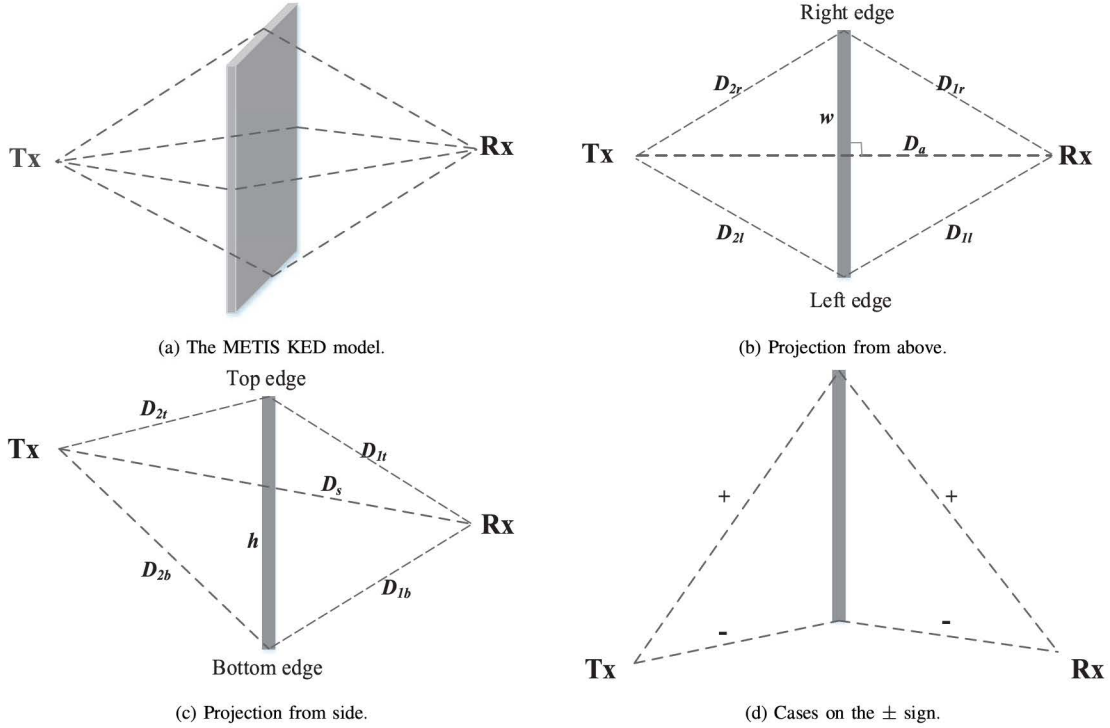


Fig. 2. (a) The METIS KED model; (b) Projection from above; (c) Projection from side; (d) Cases on the \pm sign.

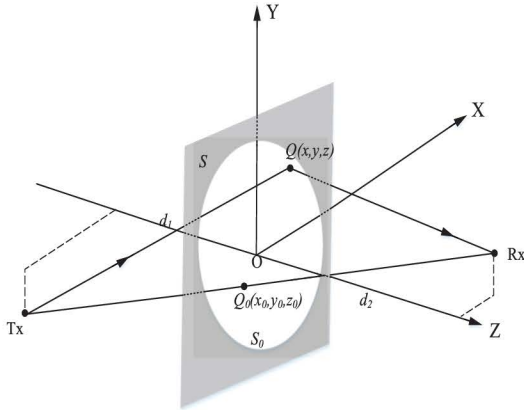


Fig. 3. Aperture diffraction for the Kirchhoff KED model.

$$A = F_d(u, v) = \frac{j}{2} \iint_{S_0} \exp[-j\frac{\pi}{2}(u^2 + v^2)] dudv \quad (4)$$

where the $F_d(u, v)$ represents the Fresnel number. The parameters u and v can be written as

$$u = \sqrt{2} \frac{x - x_0}{R_1} \quad (5)$$

$$v = \sqrt{2} \frac{y - y_0}{R_1} \quad (6)$$

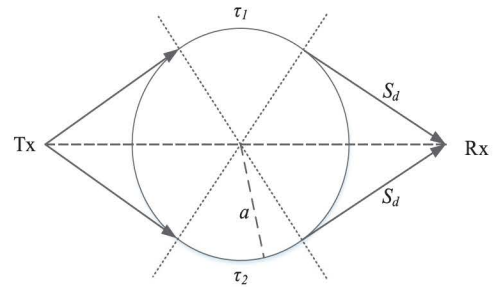


Fig. 4. The GTD model.

B. GTD Model

The GTD model simulates the human body as a perfectly conducting cylinder. The plane-wave diffraction at a circular cylinder is shown in Fig. 4.

The attenuation caused by the blockage effects is then written as [20]

$$A = \sum_{n=1}^N D_n^e \frac{\exp(-jkS_d)}{\sqrt{8jkS_d}} \times \{ \exp[-(jk + \Omega_n^e)\tau_1] + \exp[-(jk + \Omega_n^e)\tau_2] \} \quad (7)$$

where N is the selected number of zero values of Airy function $Ai(\cdot)$, k is the wavenumber, S_d is the distance between the Rx antenna and the point of tangency of the cylinder, Ω_n^e is the attenuation constant, τ_1 and τ_2 are the travel distances on the

surface of the circle for the incident rays. The parameter D_n^e is the amplitude weighting factor and can be calculated as

$$D_n^e = 2M\{Ai'(-\alpha_n)\}^{-2}e^{-\pi/6} \quad (8)$$

where $Ai'()$ is the derivative function of the Airy function $Ai()$, $-\alpha_n$ is the zeros of the Airy function $Ai()$, and the parameter M can be written as

$$M = \left(\frac{ka}{2}\right)^{1/3} \quad (9)$$

where a is the radius of the cylinder.

The attenuation constant Ω_n^e can be obtained as

$$\Omega_n^e = \frac{\alpha_n}{a} M e^{j\pi/6}. \quad (10)$$

C. Gaussian Model

The loss caused by human blockage effect when a person walks across the Tx–Rx connecting line presents a Gaussian-like shape as [11]

$$L(t) = -A_s \exp\left(-2\left((t - t_0) \frac{2}{T_s}\right)^2\right) \quad (11)$$

where A_s is the maximal loss in decibels, t_0 is the shadowing instant, T_s is the shadowing duration when the person blocks the LOS path between Tx and Rx.

IV. RESULTS AND ANALYSIS

The measurements include three cases: (1) One person walks along the Tx–Rx connecting line; (2) One person walks across the Tx–Rx connecting line; (3) Two persons walk across the Tx–Rx connecting line.

A. Case 1

The walk is shown as Path 1 in Fig.1(b). The distance between Tx and Rx is 3.6 m. A person as tall as 1.8 m and with shoulder breadth of 0.4 m walks along the line connecting the Tx and Rx antennas. The start point of the walk is 0.6 m to the Tx antenna, and the end point of the walk is 0.6 m to the Rx antenna. We measure the human blockages with a 0.2 m step.

The measurement and modeling losses for the four bands are shown in Fig. 5. The losses are between -15 dB and -30 dB. The METIS KED model and Kirchhoff KED model underestimate the losses, while the GTD model overestimates the losses. We can also see that the losses are larger as the person is near the Tx or Rx antenna.

B. Case 2

The walk is shown as Path 2 in Fig.1(b). The distance between Tx and Rx is 3 m. A person as tall as 1.8 m and with shoulder breadth of 0.4 m walks across the Tx–Rx connecting line. The distance between the Tx antenna and the cross line is 1.2 m. The distance between the person and the Tx–Rx connecting line is from -1 m to 1 m. We measure the human blockages with a 0.1 m step.

The measurement and modeling losses for the four bands are shown in Fig. 6. As can be seen, when the person walks near the Tx–Rx connecting line, the losses are severe. As the frequency increases, there is no obvious increasing trend of the losses. The METIS KED model, Kirchhoff KED model, and GTD model are used to model the losses. The Gaussian-shape is also used to fit the measurement data. The parameter

of Gaussian model for Case 2 are shown in Table I. Similar to Case 1, the METIS KED model and Kirchhoff KED model underestimate the losses, while the GTD model overestimates the losses.

TABLE I
GAUSSIAN MODEL PARAMETERS FOR CASE 2.

Frequency (GHz)	A_s (dB)	t_0 (s)	T_s (s)
11	14.14	0.01089	0.5453
16	16.19	-0.01057	0.4540
28	15.08	-0.009359	0.4842
32	14.87	-0.01508	0.5216

C. Case 3

The walk is shown as Path 3 in Fig.1(b). The distance between Tx and Rx is 4.8 m. Two persons as tall as 1.8 m and with shoulder breadth of 0.4 m walk across the Tx–Rx connecting line. The distance between the Tx antenna and the cross line near the Tx antenna is 1.2 m. The distance between the Rx antenna and the cross line near the Rx antenna is 1.2 m. The distance between the person and the Tx–Rx connecting line is from -1 m to 1 m. We measure the human blockages with a 0.1 m step.

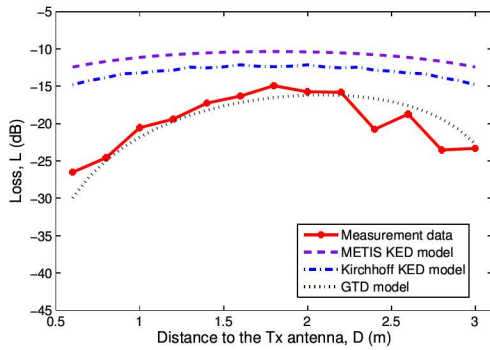
The measurement and modeling losses for the four bands are shown in Fig. 7. As there are two persons, the losses are larger compared to Case 2. The METIS KED model and Gaussian-shape are used to model the human blockage effects. The parameter of Gaussian model for Case 3 are shown in Table II. The METIS KED model can match well with the measurement data. For Case 2 and Case 3, when the person walks near the LOS path, the loss tends to be larger than 0 dB at first. This may due to that the person becomes a scatterer in the first Fresnel zone when the LOS path is not obstructed.

V. CONCLUSIONS

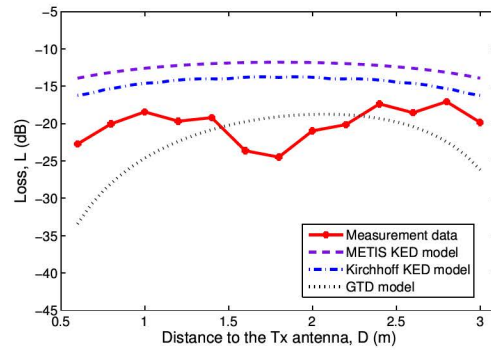
The loss caused by human body at 11, 16, 28, and 32 GHz has been investigated by measurements and modeling. Three cases of the human body blockage effects have been measured with one or two persons walking along or across the line connecting the Tx and Rx antennas. The METIS KED model, Kirchhoff KED model, and GTD model have been used to simulate the human blockage effects. The Gaussian model has also been used to fit the measurement data. The results have shown that as the frequency increases, there is no obvious increasing trend of the losses. The losses of human blockage caused by a person can be as large as 20 dB. The METIS KED model, Kirchhoff KED model, and GTD model can simulate the human blockage effects well.

ACKNOWLEDGMENT

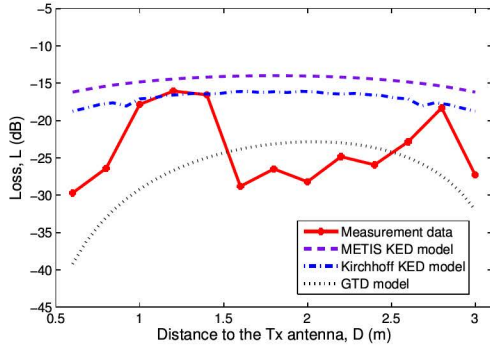
The authors would like to acknowledge the support from the EU H2020 ITN 5G Wireless project (Grant No. 641985), EU H2020 RISE TESTBED project (Grant No. 734325), EU FP7 QUICK project (Grant No. PIRSES-GA-2013-612652), and National Natural Science Foundation of China (Grant No. 61210002, 61371110).



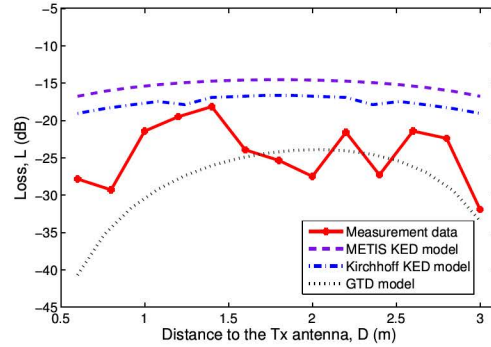
(a) Measurement and modeling losses at 11 GHz for Case 1.



(b) Measurement and modeling losses at 16 GHz for Case 1.



(c) Measurement and modeling losses at 28 GHz for Case 1.



(d) Measurement and modeling losses at 32 GHz for Case 1.

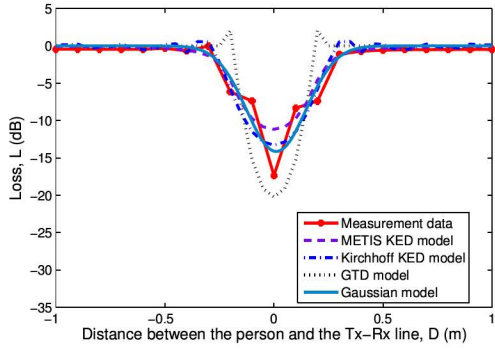
Fig. 5. Measurement and modeling losses for Case 1 at (a) 11 GHz, (b) 16 GHz, (c) 28 GHz, and (d) 32 GHz.

TABLE II
GAUSSIAN MODEL PARAMETERS FOR CASE 3.

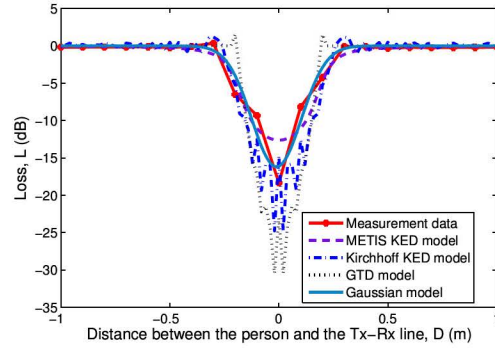
Frequency (GHz)	A_s (dB)	t_0 (s)	T_s (s)
11	30.83	-0.04472	0.4571
16	28.34	-0.02841	0.6401
28	29.21	-0.01255	0.5134
32	27.14	-0.008879	0.5473

REFERENCES

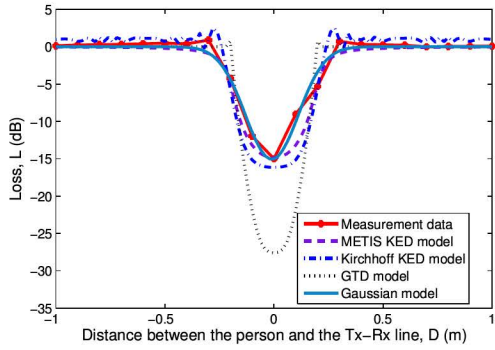
- [1] T. S. Rappaport, J. N. Murdock, and F. Gutierrez, "State of the art in 60-GHz integrated circuits and systems for wireless communications," *Proc. IEEE*, vol. 99, no. 8, pp. 1390–1436, Aug. 2011.
- [2] Z. Pi and F. Khan, "An introduction to millimeter-wave mobile broadband systems," *IEEE Commun. Mag.*, vol. 49, no. 6, pp. 101–107, Jun. 2011.
- [3] T. S. Rappaport, S. Sun, R. Mayzus, H. Zhao, Y. Azar, K. Wang, G. N. Wong, J. K. Schulz, M. Samimi and F. Gutierrez, "Millimeter wave mobile communications for 5G cellular: It will work!" *IEEE Access*, vol. 1, pp. 335–349, May 2013.
- [4] C.-X. Wang, F. Haider, X. Gao, X.-H. You, Y. Yang, D. Yuan, H. Aggoune, H. Haas, S. Fletcher, and E. Hepsaydir, "Cellular architecture and key technologies for 5G wireless communication networks," *IEEE Commun. Mag.*, vol. 52, no. 2, pp. 122–130, Feb. 2014.
- [5] X. Zhao, Q. Wang, S. Li, S. Geng, M. Wang, S. Sun, and Z. Wen, "Attenuation by human bodies at 26 and 39.5 GHz millimeter wave bands," *IEEE Antennas Wireless Propag. Lett.*, Nov. 2016.
- [6] M. Jacob, S. Priebe, A. Maltsev, A. Lomayev, V. Erceg, and T. Kürner, "A ray tracing based stochastic human blockage model for the IEEE 802.11ad 60 GHz channel model," in *Proc. EuCAP'11*, Rome, Italy, Apr. 2011, pp. 3084–3088.
- [7] M. Peter, M. Wisotzki, M. Raceala-Motoc, W. Keusgen, R. Felbecker, M. Jacob, S. Priebe, and T. Kürner, "Analyzing human body shadowing at 60 GHz: Systematic wideband MIMO measurements and modeling approaches," in *Proc. EuCAP'12*, Prague, Czech, Mar. 2012, pp. 468–472.
- [8] C. Gustafson and F. Tufvesson, "Characterization of 60 GHz shadowing by human bodies and simple phantoms," in *Proc. IEEE EuCAP'12*, Prague, Czech, Mar. 2012, pp. 473–477.
- [9] P. Karadimas, B. Allen, and P. Smith, "Human body shadowing characterization for 60 GHz indoor short-range wireless Llinks," *IEEE Antennas Wireless Propag. Lett.*, accepted for publication.
- [10] G. R. MacCartney, Jr., S. Deng, S. Sun, and T. S. Rappaport, "Millimeter-wave human blockage at 73 GHz with a simple double knife-edge diffraction model and extension for directional antennas," in *Proc. IEEE VTC'16-Fall*, Montreal, Canada, Sept. 2016.
- [11] P. Pagani and P. Pajusco, "Characterization and modeling of temporal variations on an ultrawideband radio link," *IEEE Antennas Propag.*, vol. 54, no. 11, pp. 3198–3206, Nov. 2006.
- [12] X. Wu, C.-X. Wang, J. Sun, J. Huang, R. Feng, Y. Yang, and X. Ge, "60 GHz millimeter-wave channel measurements and modeling for indoor office environments," *IEEE Trans. Antennas Propag.*, 2017, in press.
- [13] J. Huang, R. Feng, J. Sun, C.-X. Wang, W. Zhang, and Y. Yang, "Comparison of propagation channel characteristics for multiple millimeter wave bands," in *Proc. IEEE VTC'17-Spring*, Sydney, Australia, Jun. 2017, accepted for publication.
- [14] J. Huang, R. Feng, J. Sun, C.-X. Wang, W. Zhang, and Y. Yang, "Multi-frequency millimeter wave massive MIMO channel measurements and analysis," in *Proc. IEEE ICC'17*, Paris, France, May 2017, accepted for publication.
- [15] J. Huang, C.-X. Wang, R. Feng, J. Sun, W. Zhang, and Y. Yang, "Multi-frequency mmWave massive MIMO channel measurements and characterization for 5G wireless communication systems," *IEEE J. Sel. Areas Commun.*, vol. 35, no. 6, Jun. 2017, in press.
- [16] V. Nurmela et al., METIS, ICT-317669-METIS/D1.4, "METIS channel models," Jul. 2015.
- [17] M. Peter et al., mmMAGIC, H2020-ICT-671650-mmMAGIC/D2.1, "Measurement campaigns and initial channel models for preferred suitable frequency ranges," Mar. 2016.
- [18] H. D. Hristov, *Fresnel zones in wireless links, Zone Plate Lenses and Antennas*, London: Artech House, 2000.
- [19] F. P. Fontan, A. Abele, B. Montenegro, F. Lacoste, V. Fabbro, L. Castanet, B. Sanmartin, and P. Valtr, "Modelling of the land mobile satellite channel using a virtual city approach," in *Proc. EuCAP'07*, Edinburgh, UK, Nov. 2007, pp. 1–7.
- [20] G. L. James, *Geometrical theory of diffraction for electromagnetic diffraction*, 3rd edition, London: The Institution of Engineering and Technology, 1979.



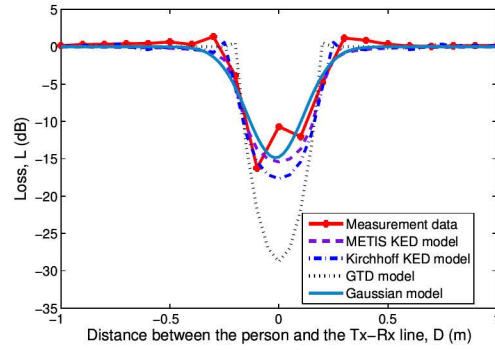
(a) Measurement and modeling losses at 11 GHz for Case 2.



(b) Measurement and modeling losses at 16 GHz for Case 2.

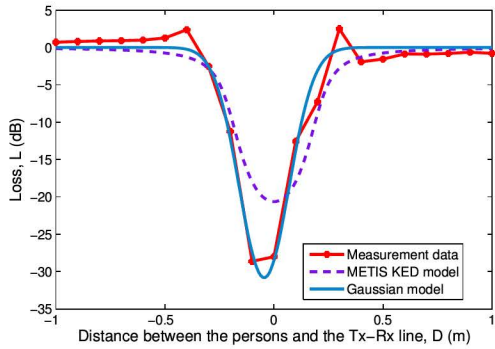


(c) Measurement and modeling losses at 28 GHz for Case 2.

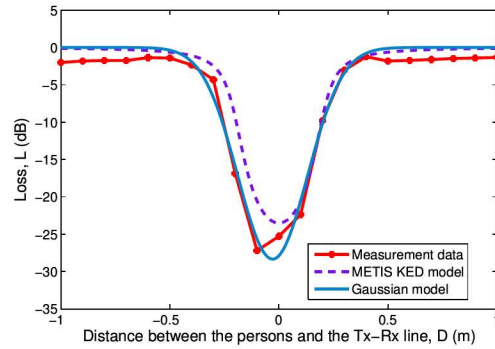


(d) Measurement and modeling losses at 32 GHz for Case 2.

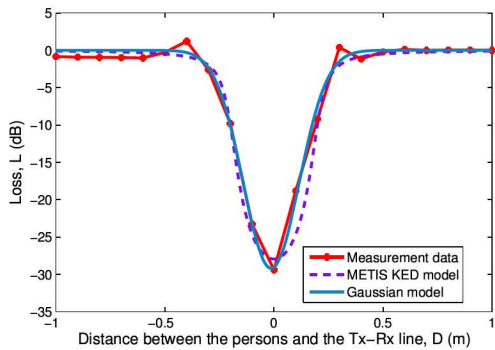
Fig. 6. Measurement and modeling losses for Case 2 at (a) 11 GHz, (b) 16 GHz, (c) 28 GHz, and (d) 32 GHz.



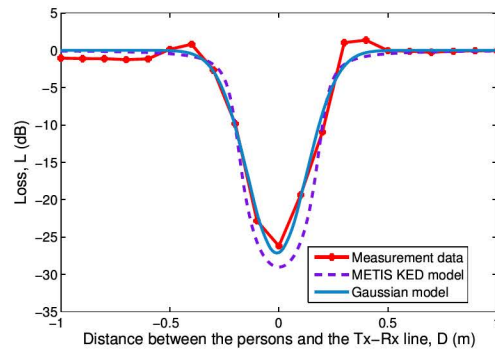
(a) Measurement and modeling losses at 11 GHz for Case 3.



(b) Measurement and modeling losses at 16 GHz for Case 3.



(c) Measurement and modeling losses at 28 GHz for Case 3.



(d) Measurement and modeling losses at 32 GHz for Case 3.

Fig. 7. Measurement and modeling losses for Case 3 at (a) 11 GHz, (b) 16 GHz, (c) 28 GHz, and (d) 32 GHz.